PCCP

PAPER

View Article Online
View Journal | View Issue

Cite this: *Phys. Chem. Chem. Phys.*, 2016, **18**, 31691

DFT studies on the heterogeneous oxidation of SO_2 by oxygen functional groups on graphene†

Guangzhi He[a] and Hong He*[abc]

The heterogeneous oxidation of SO_2 has been the subject of intense scrutiny in atmospheric chemistry because of the adverse effects of sulfate particles. Although it has been found that the soot particles with a graphene-like structure play an important role in the oxidation of SO_2, little is known about the atomic-level mechanism involved. Here, we studied the oxidation of SO_2 on oxygen-functionalized graphene using density functional theory (DFT) calculation. The results showed that SO_2 is oxidized by the epoxide group *via* a two-step mechanism, where the C–O bond away from the SO_2 is broken first, followed by the breaking of the other C–O bond and the synchronous formation of a new S–O bond. The energy barriers are significantly decreased when solvation free energies are involved, suggesting that humidity is favorable for promoting the oxidation by reducing the reaction barrier. The energy barriers for H_2SO_3 oxidation are much higher than that for SO_2 oxidation, indicating that the direct conversion of SO_2 to SO_3 is the main pathway for the oxidation of SO_2 by oxygen-functionalized graphene sheets in both the gas phase and solution. The reduced density gradient (RDG) analysis showed that the hydrogen bond formed between H_2SO_3 and epoxide groups enhances the stability of the reaction complex, and is responsible for the high energy barrier that has to be overcome for the reaction to proceed. These atomistic studies proposed a two-step mechanism for the oxidation of SO_2 on the oxygen-functionalized graphene-like carbonaceous surfaces under ambient conditions.

Received 28th September 2016,
Accepted 28th October 2016

DOI: 10.1039/c6cp06665h

www.rsc.org/pccp

1. Introduction

Sulfur dioxide (SO_2) is a global atmospheric pollutant that is generated from the combustion of sulfur-containing fossil fuels and volcanic activity, and is closely linked to many environmental and human health problems such as acid rain, haze, corrosion and respiratory diseases.[1,2] The removal and capture of SO_2 is important from both environmental and public health aspects.[3,4] On the other hand, the oxidation of SO_2 in the atmosphere results in new particle formation that is thought to play significant roles in heavy haze events.[5,6] Therefore, investigation of the heterogeneous conversion processes of SO_2 is of significant interest in atmospheric chemistry.[7]

The heterogeneous adsorption and oxidation of SO_2 on carbonaceous surfaces, including amorphous and graphene-like carbon materials, have attracted considerable attention during the past years.[8–11] It has been revealed that SO_2 molecules interact with the graphene sheets mainly *via* physisorption.[12,13] The presence of polar and oxidative functional groups may dramatically influence the electronic structure of graphene, and yields a reactive site.[14,15] The oxidation of SO_2 by graphene oxide has been observed in experiments,[16] and is demonstrated by the reduction of graphene oxide and the production of SO_4^{2-} when the reacted graphene oxide is placed in distilled water. These experimental observations motivate the theoretical investigation on the mechanism, and it has recently been found that the SO_2 molecule is oxidized by the epoxide groups on graphene oxide.[17,18] The experiments showed that the oxidation of SO_2 was more rapid in aqueous solutions,[16] and humidity can also accelerate the oxidation of SO_2.[19] However, the underlying principle is not clear, and needs to be investigated further. Under moist conditions, SO_2 can be partially converted to sulfurous acid (H_2SO_3). Therefore, the oxidation pathway of H_2SO_3 should be examined in humidity and solution environments.

Elemental carbon soot particles are ubiquitous in the lower atmosphere, which are produced from incomplete combustion processes and consist mainly of graphene sheets.[20]

[a] *State Key Joint Laboratory of Environment Simulation and Pollution Control, Research Center for Eco-Environmental Sciences, Chinese Academy of Sciences, Beijing 100085, China. E-mail: honghe@rcees.ac.cn; Fax: +86-10-62849123; Tel: +86-10-62849123*

[b] *Center for Excellence in Regional Atmospheric Environment, Institute of Urban Environment, Chinese Academy of Sciences, Xiamen 361021, China*

[c] *University of Chinese Academy of Sciences, Beijing 100049, China*

† Electronic supplementary information (ESI) available: Coordinates of the stationary points on the potential energy surface (*i.e.*, reactant complexes, transition states, intermediate, and product complexes) and results of IRC calculation. See DOI: 10.1039/c6cp06665h

Graphene sheets have been widely used as a model for the surface of porous carbon and soot to investigate the interaction (including adsorption, storage and dissociation) of various gas molecules with the graphene-like carbonaceous surfaces.[20–24] The soot particles were frequently observed to be internally mixed with sulfates in urban and marine atmospheres,[25,26] and it has been realized that the soot particles play a significant role in the oxidation of SO_2.[11,27] It can be expected that the reactive oxygen functional groups on soot surfaces resulting from combustion conditions[28,29] may be critical for the SO_2 oxidation. To elucidate the mechanism involved, an atomic-level understanding of the effect of the reactive oxygen functional groups is required.

In this work, the reaction pathways and activation barriers of the SO_2 molecule reacting with oxygen-functionalized graphene sheets were investigated by the density functional theory (DFT) calculation. The reaction pathways were traced by the intrinsic reaction coordinate (IRC) method, and the activation barriers and reaction rate constants were computed accordingly. A reduced density gradient (RDG) analysis was carried out to interpret the origin of the difference in barrier height between the reactions starting from SO_2 and H_2SO_3. The electronic localization function (ELF) and Mayer bond order were used to characterize the bond breaking and formation during the reaction process.

2. Computational methods

The M06-2X functional[30] and 6-311G(d,p) basis set were used for unconstrained geometry optimization and transition state searches. Vibrational frequency calculations were carried out at the same level to identify the minima and transition states on the potential energy surface and to estimate the thermal correction to the Gibbs free energy. To confirm the transition states and their connected minima, intrinsic reaction coordinate (IRC) calculations[31] were performed to follow the reaction pathways. Coordinates of the stationary points on the potential energy surface and results of the IRC calculations are presented in the ESI.† To improve the accuracy of electronic energies, single-point energies at converged geometries were evaluated at the M062X/6-311+G(2df,2p) level using the DFT-D3 method.[32] The interaction energies between the sulfur oxide molecules and graphene were calculated at this level using the counterpoise procedure to correct the basis-set superposition error (BSSE).[33] The SMD solvation model was used to represent the solvent in terms of its average effect on the solute and to compute the aqueous solvation free energies at the M052X/6-31G(d) level.[34] The solvation free energy is defined as[35]

$$\Delta G_{solv} = E_{sol} - E_{gas} \quad (1)$$

where E_{sol} and E_{gas} refer to the electronic energy in the presence and absence of the continuum solvent field. All the DFT calculations were performed using the Gaussian 09 package.[36]

We applied the conventional transition state theory formula, including the Wigner tunneling correction, to calculate the reaction rate constant [eqn (2)] using the KiSThelP code,[37] where χ is the Wigner transmission coefficient [eqn (3)], k_B is the Boltzmann constant, h is the Planck constant, T is the temperature, $\mathrm{Im}(\nu^{\neq})$ is the imaginary frequency, and ΔG is the difference in Gibbs free energies between the transition state in each pathway and the reactant complex.

$$k = \chi \frac{k_B T}{h} \exp\left(-\frac{\Delta G}{k_B T}\right) \quad (2)$$

$$\chi = 1 + \frac{1}{24}\left(\frac{h\mathrm{Im}(\nu^{\neq})}{k_B T}\right)^2 \quad (3)$$

The electron localization function (ELF),[38] reduced density gradient (RDG),[39] and Mayer bond order were analyzed using the Multiwfn package.[40] Geometries and the isosurface of RDG(r) were visualized using VMD software.[41]

3. Results and discussion

3.1. Reaction pathway

Schematic reaction pathways including Gibbs free energies at 298 K and 1 atm as well as the optimized geometries of the reactants, transition states, intermediates, and products are shown in Fig. 1 and 2. The oxygen-functionalized graphene sheet was modeled using a polycyclic $C_{80}H_{22}$ planar cluster with one oxygen functional group (stabilized at the epoxide structure) at the center of the basal plane. Due to the size and edge effects, the properties estimated using the finite-size model may vary from those of the real system to some extent. However, it can be expected that the results obtained with the current model would be qualitatively reliable in predicting the chemical processes occurring in the local region of graphene oxide surfaces.

Our DFT calculation showed that the oxidation of SO_2 proceeds *via* two steps. When the SO_2 molecule approached the epoxide group, the C–O bond away from the SO_2 broke first and formed an intermediate. Then, the SO_2 molecule got closer to the surface oxygen group, synchronized with the breaking of the other C–O bond, leading to the final formation of a SO_3 molecule. The overall energy barrier for this pathway is 17.8 kcal mol^{-1} in the gas phase. This activation barrier is below 21 kcal mol^{-1}, which is surmountable at room temperature,[42] suggesting that the oxidation of SO_2 by surface epoxide groups can occur under ambient conditions. This process is exothermic by 42.1 kcal mol^{-1}. From the analysis of the activation barriers of the two steps, the rate-limiting step in the oxidation is the breaking of the first C–O bond, and the subsequent process of the second C–O bond breaking and the S–O bond formation is, instead, very fast due to the rather low energy barrier (2.0 kcal mol^{-1}).

It is notable that the overall energy barrier is significantly decreased to 9.2 kcal mol^{-1} when aqueous solvation free energies are involved (see Fig. 1), suggesting that the oxidation of SO_2 can be promoted in humidity and solution environments. This result is qualitatively consistent with the experimental observation.[16] The higher the polarity, the more the energy is reduced by the solvation effect. Therefore, the promotion mechanism is attributed to a higher polarity of the transition state relative to the reactant.

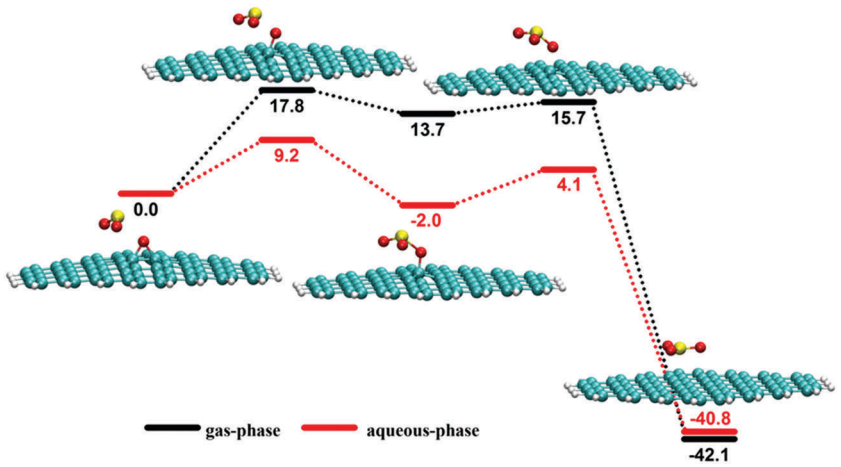

Fig. 1 Energy profile of the reaction pathway of SO_2 oxidation by the oxygen-functionalized graphene sheet. Gibbs free energies are given in kcal mol^{-1} relative to the reactant complex. Red, yellow, blue, and white circles denote O, S, C, and H atoms, respectively.

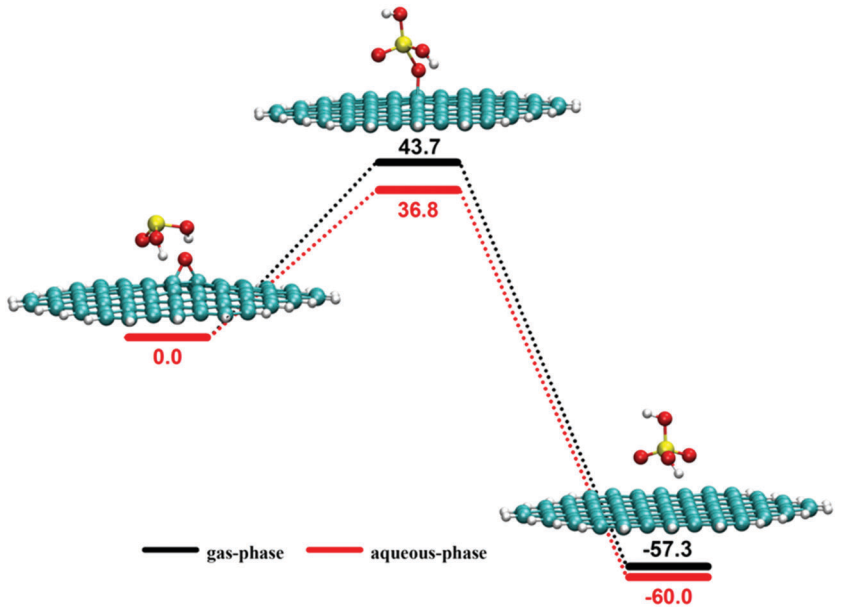

Fig. 2 Energy profile of the reaction pathway of H_2SO_3 oxidation by the oxygen-functionalized graphene sheet. The units of energy and the color legend are the same as that of Fig. 1.

In a moist environment, some SO_2 can be converted to sulfurous acid (H_2SO_3). An alternative oxidation pathway may start with H_2SO_3. This process was found to be a simple one-step reaction (see Fig. 2). The energy barriers are 43.7 kcal mol^{-1} in the gas phase and 36.8 kcal mol^{-1} in the aqueous phase, both of which are significantly higher than that for the conversion of SO_2 to SO_3 and are prohibitive under normal conditions. Therefore, this pathway is unlikely to proceed at room temperature.

According to the energies of the activation barriers, the rate constants for the two pathways can be calculated through transition state theory.[37] At room temperature (298 K), under gas-phase conditions, we obtain the overall rate constant of 6.8×10^{-1} s^{-1} for SO_2 oxidation, whereas the rate constant for H_2SO_3 oxidation is only 8.1×10^{-20} s^{-1}, showing that the oxidation of SO_2 is favored over the oxidation of H_2SO_3 by a factor of 8.4×10^{18}. In the aqueous phase, the rate constants are increased to 1.4×10^{6} s^{-1} and 9.0×10^{-15} s^{-1} for the oxidation of SO_2 and H_2SO_3, respectively, yielding a ratio of 1.6×10^{20}. This result indicates that the direct conversion of SO_2 to SO_3 would be the main pathway for SO_2 oxidation by oxygen-functionalized graphene sheets in both the gas phase and solution.

3.2. Interaction properties of reactant and product complexes

To interpret the origin of the difference in barrier height between the reactions starting from SO_2 and H_2SO_3, the reduced density gradient of the electron density [RDG(r)], defined as $|\nabla\rho(r)/\rho^{4/3}(r)|$, was analyzed. RDG($r$) is a very efficient method for describing weak interactions, including hydrogen bonding, van der Waals force,

and steric effects.[39,43] The isosurface of RDG(r) mapped by a colored $\Lambda(r)$ parameter is capable of visually revealing not only the region of weak interaction, but also the type and strength. The $\Lambda(r)$ parameter denotes Sign[$\lambda_2(r)$]$\rho(r)$, where λ_2 is the second largest eigenvalue of a Hessian matrix of the electron density.

As shown in Fig. 3a, there is a significant green region between the SO_2 molecule and the oxygen-functionalized graphene sheet, clearly indicating that the principal stabilizing component for the reactant complex of SO_2 is the van der Waals attraction. The calculated interaction energy of SO_2 with the substrate is 7.3 kcal mol^{-1}. However, the reaction complex of H_2SO_3 is stabilized by hydrogen bonding (see the blue isosurface between the epoxide group and the H atom of H_2SO_3 in Fig. 3c) and van der Waals attraction together. The corresponding interaction energy is 12.8 kcal mol^{-1}, much stronger than that of the SO_2 reactant complex. The higher stability of the reactant complex leads to a higher energy barrier that has to be overcome for the reaction to proceed. The results of RDG analysis and interaction energies indicate that the strong attraction from hydrogen bonding is responsible for the high degree of stabilization of the H_2SO_3 reactant complex and hence the high energy barrier that has to be overcome.

RDG analysis also verifies that the products of the two reaction pathways (*i.e.*, SO_3 and H_2SO_4) are physisorbed on the graphene sheet mainly through van der Waals attraction (Fig. 3b and d). The corresponding interaction energies are 8.3 and 9.0 kcal mol^{-1}, respectively. The small yellowish regions shown in Fig. 3a–d suggest the coexistence of a weak repulsion. The red spindle-shaped isosurfaces show the strong steric repulsion in the inner region of the aromatic ring.

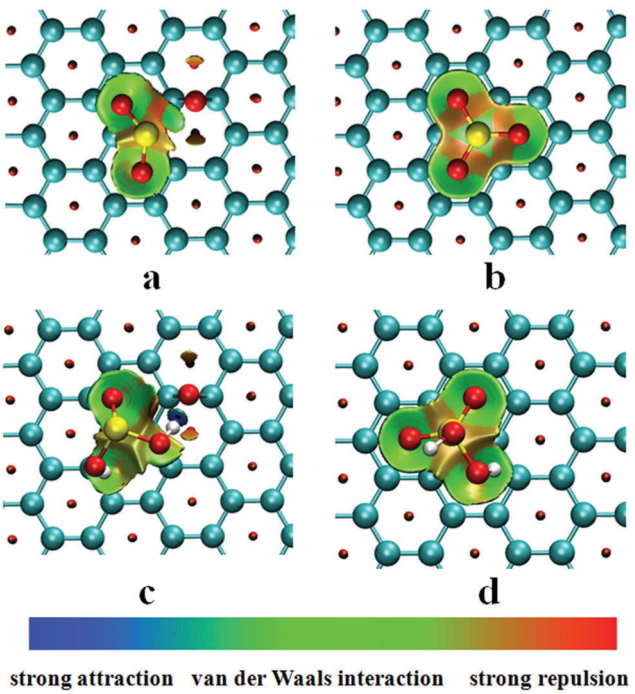

Fig. 3 RDG isosurfaces are colored to show the values of Sign[$\lambda_2(r)$]$\rho(r)$: (a) and (b) are the reactant and product complexes for the reaction starting from SO_2; (c) and (d) are the reactant and product complexes for the reaction starting from H_2SO_3. The color bar shows the blue-green-red scale ranging from −0.04 to 0.02 a.u. Blue, green, and red represent the strong attraction (*e.g.*, hydrogen bonding), van der Waals interaction, and strong repulsion, respectively. Areas beyond the interaction are omitted for clarity.

3.3. Transformation of bonding structures during reaction

In order to clearly identify the change in the chemical bonding character during the reaction process, electronic localization function (ELF) analysis was performed for the minima and transition states along the pathway of SO_2 reacting with the oxygen-functionalized graphene sheet (see Fig. 4). ELF = 1 corresponds to perfect electron localization, while ELF = 0 denotes a completely delocalized situation. A high value of ELF at a given point represents the existence of covalent bonds, lone pairs, or core electrons therein.[38,44] Regions of the greatest and the smallest localization electron density are represented by red and blue colors, respectively. The O atom of the epoxide group is named O1, and the two C atoms bonded to O1 on graphene are named C1 and C2, respectively (see Fig. 5).

In the first reaction step, from the reactant complex to the intermediate, the ELF value between the S atom and the O1 atom increases from about 0.05 to 0.60 (Fig. 4a–c) as the S–O1 distance decreases from 2.75 Å to 1.91 Å (Fig. 5), indicating that the electrons begin to locally concentrate between the two atoms. Meanwhile, the C1–O1 distance is lengthened from 1.43 Å to 2.23 Å, and the corresponding ELF value is significantly decreased from about 0.85 to 0.40, which suggests that the C1–O1 bond is being broken in the intermediate species. The ELF analysis clearly shows that the S atom and the O1 atom begin to interact with each other and the C1–O1 bond is broken during the first reaction step.

After the breaking of the C1–O1 bond, SO_2 may continue to attack the surface O species from the intermediate. As the electron density between the S atom and the O1 atom is further increased, the two atoms show a strong covalent interaction (ELF value = 0.85, Fig. 4f), which decreases the S–O1 distance to 1.43 Å when this half-reaction ends at the product complex. The Mayer bond order analysis corroborates the formation of the new covalent S–O1 bond with a significant value of 1.71 (Fig. 5). On the other hand, further interaction between the S atom and the O1 atom enhances the delocalization between the O1 atom and the C2 atom (ELF value = 0). As a result, the C2–O1 bond is completely broken, at a distance of 3.24 Å. The ELF maps shown in Fig. 4d–f show that there is a high degree of synchronization of C2–O1 bond breaking with S–O1 bond formation in the second reaction step.

As shown in Fig. 5, the higher the ELF value, the higher the Mayer bond order. The ELF value and Mayer bond order increase with the decrease of the corresponding atomic distance, and *vice versa*. Both ELF analysis and Mayer bond order describe well the C–O bond breaking and the S–O bond formation processes in the reaction. The natural population analysis (NPA) shows that the NPA charge of the S atom increases from +1.61 to +2.41 during the reaction (Fig. 5), suggesting that the electrons transfer from the S atom to the O atom and result in the oxidation of SO_2 to SO_3.

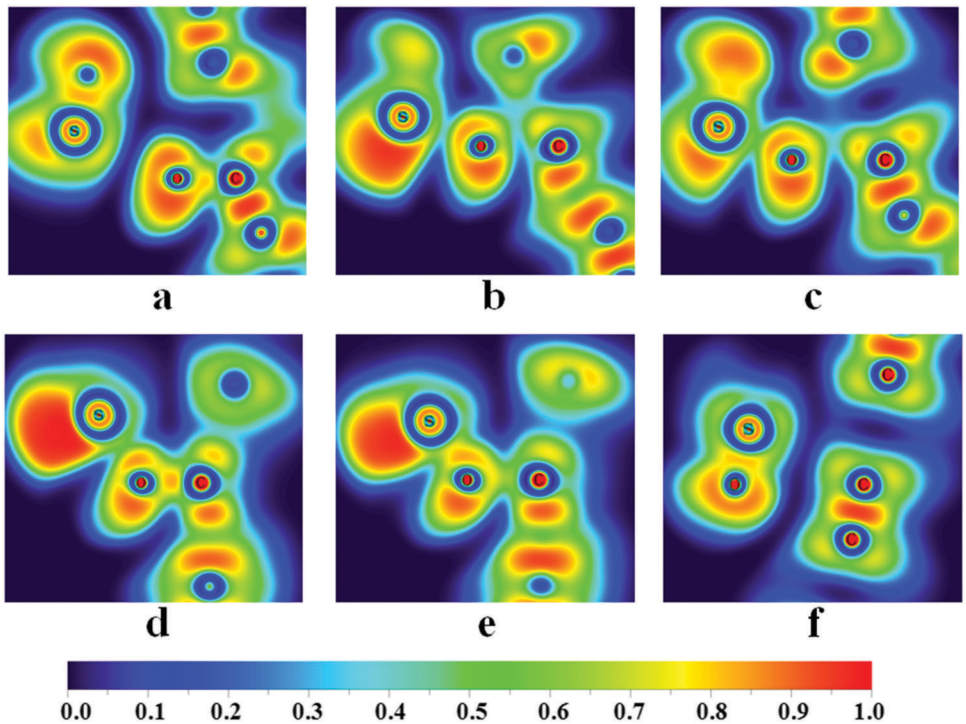

Fig. 4 The two-dimensional electron localization function (ELF) color-filled maps of SO_2 reacting with the oxygen-functionalized graphene sheet: (a–c) the ELF maps of the reactant complex, first transition state, and intermediate in the C1–O1–S plane; (d–f) the ELF maps of the intermediate, second transition state, and product complex in the C2–O1–S plane. Areas beyond the interaction are omitted for clarity.

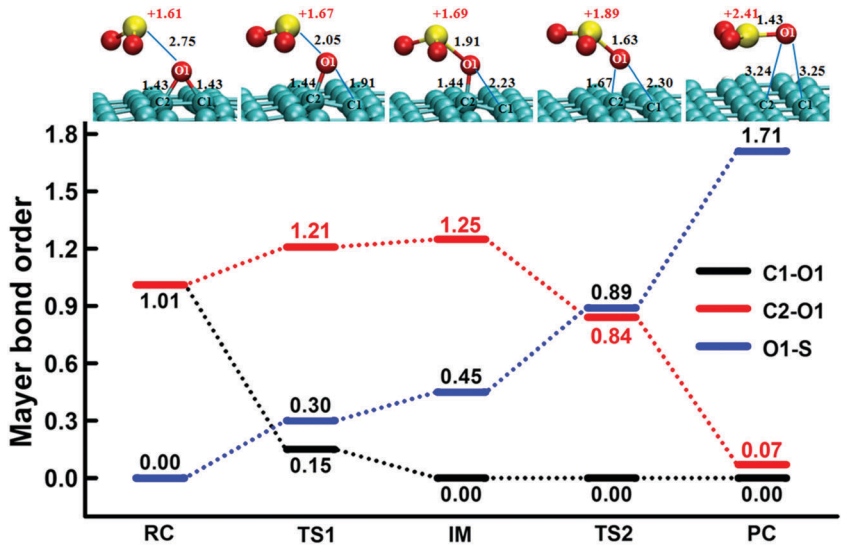

Fig. 5 Atomic distance, Mayer bond order, and natural population analysis (NPA) charges for the minima and transition states along the pathway of SO_2 reacting with the oxygen-functionalized graphene sheet. RC: reactant complex; TS1: the first transition state; IM: intermediate species; TS2: the second transition state; PC: product complex. The Mayer bond order lower than the default threshold of 0.05 is regarded as zero. All lengths are given in Å.

4. Conclusions

The DFT-calculated results in this study indicate that epoxide groups on the graphene sheet are able to oxidize SO_2 at room temperature, and the solvation effect can promote the oxidation by reducing the reaction barrier, which explained theoretically the experimental observation.[16] A two-step oxidation mechanism was identified based on the DFT-calculated reaction pathway and the detailed picture of bond breaking and bond formation along the reaction pathway. The energy barrier for H_2SO_3 oxidation is predicted to be significantly higher than that for SO_2 oxidation, indicating that the direct conversion of SO_2 to SO_3 would be the main pathway for the oxidation of SO_2 by oxygen-functionalized graphene sheets.

The present work implies that the oxidation of SO_2 on oxygen-functionalized graphene-like carbonaceous materials such as soot may occur extensively. The oxidation of SO_2 in the atmosphere results in new particle formation that is thought to play significant roles in heavy haze events. Therefore, this work could help enhance our understanding of the atmospheric sulfur cycle. The mechanism described here may also provide new insights into developing a cost-effective and efficient approach for SO_2 removal that is based on direct oxidation at the gas–solid interface and requires no additional oxidants, because conventional flue gas desulfurization (FGD) methods require high energy consumption.[45]

Acknowledgements

This work was supported by the Strategic Priority Research Program of the Chinese Academy of Sciences (XDB05010300) and the National Natural Science Foundation of China (91543109). We thank the National Supercomputing Center in Shenzhen for providing computing resources and the Gaussian 09 program.

References

1 H. Bao, S. Yu and D. Q. Tong, *Nature*, 2010, **465**, 909–912.
2 K. Wark, C. F. Warner and W. T. Davis, *Air Pollution: Its Origin and Control*, Addison-Wesley, 1998.
3 R. K. Srivastava and W. Jozewicz, *J. Air Waste Manage. Assoc.*, 2001, **51**, 1676–1688.
4 C. Wang, G. Cui, X. Luo, Y. Xu, H. Li and S. Dai, *J. Am. Chem. Soc.*, 2011, **133**, 11916–11919.
5 M. Kulmala, U. Pirjola and J. M. Makela, *Nature*, 2000, **404**, 66–69.
6 H. He, Y. Wang, Q. Ma, J. Ma, B. Chu, D. Ji, G. Tang, C. Liu, H. Zhang and J. Hao, *Sci. Rep.*, 2014, **4**, 4172.
7 E. Harris, B. Sinha, D. van Pinxteren, A. Tilgner, K. W. Fomba, J. Schneider, A. Roth, T. Gnauk, B. Fahlbusch, S. Mertes, T. Lee, J. Collett, S. Foley, S. Borrmann, P. Hoppe and H. Herrmann, *Science*, 2013, **340**, 727–730.
8 A. S. Rad, M. Esfahanian, S. Maleki and G. Gharati, *J. Sulfur Chem.*, 2016, **37**, 176–188.
9 M. Seredych and T. J. Bandosz, *J. Phys. Chem. C*, 2010, **114**, 14552–14560.
10 Y. W. Lee, J. W. Park, J. H. Choung and D. K. Choi, *Environ. Sci. Technol.*, 2002, **36**, 1086–1092.
11 T. Novakov, S. G. Chang and A. B. Harker, *Science*, 1974, **186**, 259–261.
12 L. Shao, G. Chen, H. Ye, Y. Wu, Z. Qiao, Y. Zhu and H. Niu, *Eur. Phys. J. B*, 2013, **86**, 54.
13 J. L. Llanos, A. E. Fertitta, E. S. Flores and E. J. Bottani, *J. Phys. Chem. B*, 2003, **107**, 8448–8453.
14 E. C. Mattson, K. Pande, M. Unger, S. Cui, G. Lu, M. Gajdardziska-Josifovska, M. Weinert, J. Chen and C. J. Hirschmugl, *J. Phys. Chem. C*, 2013, **117**, 10698–10707.
15 S. Tang and Z. Cao, *J. Phys. Chem. C*, 2012, **116**, 8778–8791.
16 Y. Long, C. Zhang, X. Wang, J. Gao, W. Wang and Y. Liu, *J. Mater. Chem.*, 2011, **21**, 13934–13941.
17 H. J. Zhang, W. L. Cen, J. Liu, J. X. Guo, H. Q. Yin and P. Ning, *Appl. Surf. Sci.*, 2015, **324**, 61–67.
18 W. L. Cen, M. L. Hou, J. Liu, S. D. Yuan, Y. J. Liu and Y. H. Chu, *RSC Adv.*, 2015, **5**, 22802–22810.
19 V. Gaur, R. Asthana and N. Verma, *Carbon*, 2006, **44**, 46–60.
20 A. Rodriguez-Fortea, M. Iannuzzi and M. Parrinello, *J. Phys. Chem. C*, 2007, **111**, 2251–2258.
21 A. M. Kamat, A. C. T. van Duin and A. Yakovlev, *J. Phys. Chem. A*, 2010, **114**, 12561–12572.
22 A. Rodriguez-Fortea and M. Iannuzzi, *J. Phys. Chem. C*, 2008, **112**, 19642–19648.
23 C. Garcia-Fernandez, S. Picaud, M. T. Rayez, J. C. Rayez and J. Rubayo-Soneira, *J. Phys. Chem. A*, 2014, **118**, 1443–1450.
24 I. Cabria, M. J. López, S. Fraile and J. A. Alonso, *J. Phys. Chem. C*, 2012, **116**, 21179–21189.
25 M. Posfai, J. R. Anderson, P. R. Buseck and H. Sievering, *J. Geophys. Res.: Atmos.*, 1999, **104**, 21685–21693.
26 A. Meszaros and E. Meszaros, *Aerosol Sci. Technol.*, 1989, **10**, 337–342.
27 B. Zheng, Q. Zhang, Y. Zhang, K. B. He, K. Wang, G. J. Zheng, F. K. Duan, Y. L. Ma and T. Kimoto, *Atmos. Chem. Phys.*, 2015, **15**, 2031–2049.
28 C. Han, Y. Liu, C. Liu, J. Ma and H. He, *J. Phys. Chem. A*, 2012, **116**, 4129–4136.
29 J. P. Cain, P. L. Gassman, H. Wang and A. Laskin, *Phys. Chem. Chem. Phys.*, 2010, **12**, 5206–5218.
30 Y. Zhao and D. G. Truhlar, *Theor. Chem. Acc.*, 2008, **120**, 215–241.
31 K. Fukui, *Acc. Chem. Res.*, 1981, **14**, 363–368.
32 S. Grimme, J. Antony, S. Ehrlich and H. Krieg, *J. Chem. Phys.*, 2010, **132**, 154104.
33 S. F. Boys and F. Bernardi, *Mol. Phys.*, 2002, **100**, 65–73.
34 A. V. Marenich, C. J. Cramer and D. G. Truhlar, *J. Phys. Chem. B*, 2009, **113**, 6378–6396.
35 J. Ho, A. Klamt and M. L. Coote, *J. Phys. Chem. A*, 2010, **114**, 13442–13444.
36 M. J. Frisch, G. W. Trucks, H. B. Schlegel, G. E. Scuseria, M. A. Robb, J. R. Cheeseman, G. Scalmani, V. Barone, B. Mennucci, G. A. Petersson, H. Nakatsuji, M. Caricato, X. Li, H. P. Hratchian, A. F. Izmaylov, J. Bloino, G. Zheng, J. L. Sonnenberg, M. Hada, M. Ehara, K. Toyota, R. Fukuda, J. Hasegawa, M. Ishida, T. Nakajima, Y. Honda, O. Kitao, H. Nakai, T. Vreven, J. A. Montgomery, Jr., J. E. Peralta, F. Ogliaro, M. Bearpark, J. J. Heyd, E. Brothers, K. N. Kudin, V. N. Staroverov, R. Kobayashi, J. Normand, K. Raghavachari, A. Rendell, J. C. Burant, S. S. Iyengar, J. Tomasi, M. Cossi, N. Rega, N. J. Millam, M. Klene, J. E. Knox, J. B. Cross, V. Bakken, C. Adamo, J. Jaramillo, R. Gomperts, R. E. Stratmann, O. Yazyev, A. J. Austin, R. Cammi, C. Pomelli, J. W. Ochterski, R. L. Martin, K. Morokuma, V. G. Zakrzewski, G. A. Voth, P. Salvador, J. J. Dannenberg, S. Dapprich, A. D. Daniels, O. Farkas, J. B. Foresman, J. V. Ortiz, J. Cioslowski and D. J. Fox, *Gaussian09, Revision D.01*, Gaussian, Inc., Wallingford CT, 2009.
37 S. Canneaux, F. Bohr and E. Henon, *J. Comput. Chem.*, 2014, **35**, 82–93.

38 A. D. Becke and K. E. Edgecombe, *J. Chem. Phys.*, 1990, **92**, 5397–5403.
39 E. R. Johnson, S. Keinan, P. Mori-Sanchez, J. Contreras-Garcia, A. J. Cohen and W. Yang, *J. Am. Chem. Soc.*, 2010, **132**, 6498–6506.
40 T. Lu and F. Chen, *J. Comput. Chem.*, 2012, **33**, 580–592.
41 W. Humphrey, A. Dalke and K. Schulten, *J. Mol. Graphics Modell.*, 1996, **14**, 33–38.
42 D. C. Young, *Computational Chemistry: A Practical Guide for Applying Techniques to Real-World Problems*, John Wiley & Sons, Inc., New York, 2002, ch. 17, pp. 147–158.
43 J. Miao, B. Song and Y. Gao, *Chem. – Eur. J.*, 2016, **22**, 2586–2589.
44 X. Li, *J. Mol. Model.*, 2012, **18**, 1003–1008.
45 H. Wu, W. Cai, M. Long, H. Wang, Z. Wang, C. Chen, X. Hu and X. Yu, *Environ. Sci. Technol.*, 2016, **50**, 5809–5816.